ADVANCED OPTICAL MATERIALS
www.advopticalmat.de

Numerical Aperture Dependence of Mie Modes in Low Refractive Index Particles and Enhanced Collection Using Metallic Substrates

*Sunny Tiwari and Tristan Farrow**

Advancements in utilizing low refractive index dielectric particles have implications for sensing, lasing, and strong-coupling at nano and microscopic scales. These cavities offer benefits like ease of fabrication and biocompatibility, making them promising for a wide range of technologies by utilizing their narrow linewidth modes. However, optical modes sustained in these dispersive systems can show distinct behaviors depending on the detection configuration. This study shows the influence of numerical aperture (NA) of the objective lens on the detection of Mie modes in a dielectric microsphere under far-field excitation and collection. It is demonstrated experimentally and numerically that Mie modes from microspheres outcouple at different angles, with variations in mode amplitudes contingent on the NA of the objective lens, thus leading to distinct linewidths while probing with different NA objectives. Furthermore, it is shown that metallic substrates can facilitate efficient detection of Mie modes by redirecting scattered modes towards low angles. This enables mode detection with low NA lenses and further preventing the inclusion of incident scattered light from higher angles which otherwise perturb the modes. The results underline the importance of careful detection strategies to fully harness dielectric particles as optical platforms for applications in particle detection and characterization.

1. Introduction

Dielectric cavities are highly promising for lasing,[1,2] sensing,[3] and nanophotonic applications[4–7] due to their ease of fabrication, biocompatibility,[8,9] and scalability.[10–13] Depending on the geometry and method of excitation, these cavities support high-finesse optical modes such as whispering gallery modes (WGMs)[14,15] and Mie resonances. WGMs have widespread use in applications like diffraction limited imaging,[16–18] lasing,[19–22] and vectorial beam generation.[23] Unlike WGMs emission, which is inherently non-directional, Mie modes in resonators with size larger than the wavelength of the light is directional in nature.[24] This can have implications for coupling to integrated photonic elements on-chip where directionality of light is essential. Mie resonances, particularly in small high-refractive-index particles, are key for subwavelength optics, to enable light manipulation in devices such as optical antennas[25] and photonic metamaterials.[26,27] Unlike high-refractive-index particles, which exhibit significant losses, low refractive-index particles have minimal losses, making them more suitable for practical applications in nanospectroscopy[28] due to the ability to route emission directionally and to achieve sub-diffraction lateral resolution in imaging[29] by utilizing the photonic nanojet effect.[30] In addition, they have been utilized in the enhancement and directional control of fluorescence and surface enhanced Raman scattering.[23,31,32] However, due to their low refractive index contrast, dielectric nanoparticles with low refractive indices exhibit weak resonances albeit, attempts have been made to observe Mie resonances in such materials.[33]

Larger, low-refractive-index microspheres can also sustain high quality factor modes and have wide implications in super-resonance effect,[34] high order Fano resonances,[35] probing strong light–matter interaction facilitated by the sharp resonances at visible wavelengths.[36,37] The larger surface area of microspheres onto which molecular layers can be coated and their emission coupled to the cavity modes[38,39] gives them an advantage of open optical cavities. However, observing Mie modes in dispersive optical geometries, such as microresonators, may lead to variability in linewidth, depending on the detection scheme.[40] This type of dependency of linewidth and profile of modes collected from metallic nanoparticles is also studied in detail[41] and technique such as near normal incidence

S. Tiwari, T. Farrow
Department of Physics
University of Oxford
Parks Road, Oxford OX1 3PU, UK
E-mail: tristan.farrow@cantab.net
T. Farrow
NEOM
Education, Research, and Innovation sector
Tabuk 49643-9136, Saudi Arabia

The ORCID identification number(s) for the author(s) of this article can be found under https://doi.org/10.1002/adom.202501451

DOI: 10.1002/adom.202501451

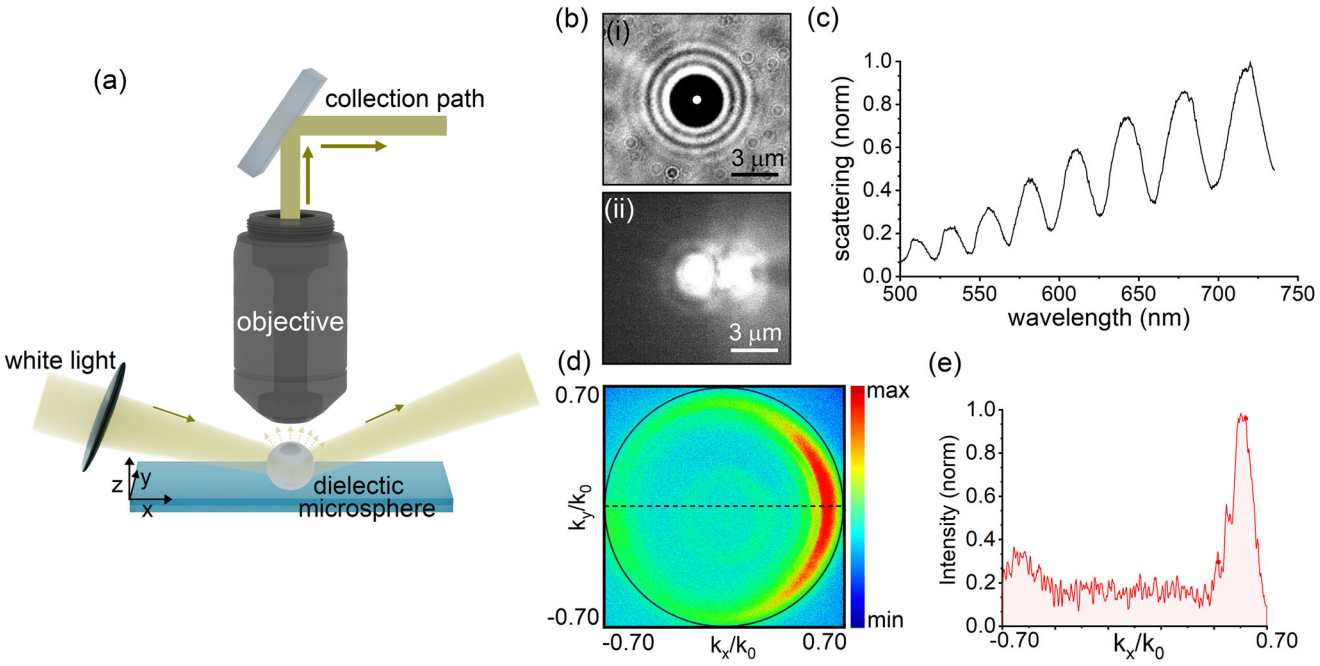

Figure 1. Schematic of the experimental configuration. a) A dielectric microsphere (3μm) placed on a glass substrate was illuminated using a loosely focused white light at an oblique angle. The scattered light was collected using a dry objective lens and was routed to the spectrometer or to the camera for real and Fourier plane imaging. b,i) Transmission image of the microsphere. ii) Bright field image of the same microsphere under oblique angle excitation showing the preferred scattering of light along the direction of excitation light. c) Mie spectrum of the light scattered from the microsphere. d) Fourier plane image of the scattered light. e) Intensity cross-cut of the Fourier plane image along the black dotted line (along $k_y/k_0 = 0$) showing the confinement of scattered light at higher angles along the direction of the excitation light.

dark field microscopy[42] has been proposed to probe resonances with better accuracy. While the effect of detection configuration on WGMs linewidths in low refractive index particles is well-studied and discussed in terms of optical bending[43] and geometric eccentricity,[44] probing Mie resonances also require further exploration under far-field excitation and detection configuration.

Herein, we perform experimental and numerical studies to show that Mie modes in low refractive index microspheres exhibit angular dependent outcoupling under far-field oblique excitation and collection, a general configuration used in dark-field spectroscopy. Using momentum-resolved and dark-field spectroscopy, we show that low NA objective lenses are unable to efficiently collect Mie modes scattered at higher angles, leading to broadened or diminished resonances. We show that this can be mitigated by utilizing metallic substrates, which act as optical antenna to enhance and redirect the scattered wavevectors of Mie modes of microspheres, and higher order modes in nanospheres, toward lower collection angles. The results provide important insight into the dependence of detection configuration on perceived Mie scattering linewidths and offer a methodology to optimize the performance of dielectric microsphere and nanosphere based optical platforms for nanophotonic applications.

2. Results and Discussion

A dielectric SiO_2 microsphere of diameter 3μm placed on a glass substrate (**Figure 1a**) was illuminated using a loosely focused white light at an oblique angle of 20° with respect to the substrate and the scattered light was collected using a dry 60×, 0.70 NA objective lens (see Supporting Information S1 and S2 for details on sample preparation and experimental setup). The collected light was then routed to the spectrometer for spectroscopy and to the imaging camera to perform bright field and Fourier plane imaging. The microsphere was imaged and located on the substrate using collimated white light in the transmission imaging configuration (Figure 1b(i)). Upon excitation with the white light under oblique angle incidence, the microsphere scatters light preferably along the direction of the incident light (shown in Figure 1b(ii)). Figure 1c shows Mie spectrum from the microsphere with resonant optical modes arising when light interacts with particles of a size comparable to or larger than the wavelength of the light. We later show that these observed modes depend strongly on the collection numerical aperture. The Mie modes are characterised by the orbital (l) and azimuthal (m) mode numbers and can have either transverse electric (TE) or transverse magnetic (TM) polarizations. Figure 1d shows the Fourier plane image of the scattered light from the microsphere. The light is scattered at higher angles in the direction of the incoming light, which is the characteristic of the Mie scattering as it is directional in nature.[24] The intensity cross-cut (Figure 1e) along the black dotted line in the Fourier image plane (along $k_y/k_0 = 0$) in Figure 1d shows the confinement of the scattered light at higher angles. This shows that in the far-field excitation regime, using slant angle excitation, the generated Mie scattering modes are more confined at higher angles.

To show the effect of the collection angles on the perceived linewidth of the Mie modes, we performed numerical

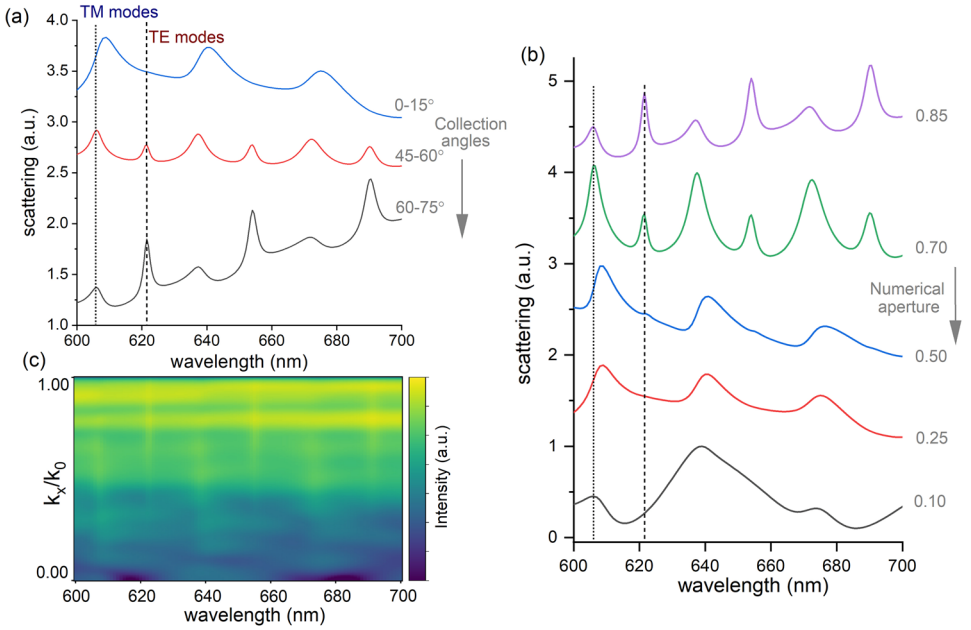

Figure 2. Numerically calculated Mie scattering spectra from a 3μm microsphere placed on a glass substrate upon illumination at an angle of 20° with respect to the substrate. a) Variation of observed mode linewidths for a collection angular range of 0°–15°, 45°–60°, and 60°–75°. For smaller collection angles, the linewidth of the observed modes are very broad whereas for light scattered along larger angles the modes are sharper. b) Variation of the mode linewidth as a function of the numerical aperture of the detection optics. c) Energy-momentum image showing the gradual variation of the mode linewidth as a function of the scattered wavevectors.

calculations using SMUTHI,[45] an open-source Python package that solves three-dimensional Maxwell's equations in the frequency domain. It employs the T-matrix method to address light scattering problems by expanding the scattered electromagnetic field from a particle on a substrate into outgoing spherical vector wave functions.[46] The numerical accuracy is determined by the truncation order of the spherical wave (multipole) expansion. A higher truncation order includes more multipole terms, capturing finer resonances and angular features, while a lower order may miss higher order modes and lead to inaccurate results. For larger particles (diameter of particle > wavelength of light), increasing the maximum multipole order improves accuracy and ensures convergence of the solution. The methodology of ensuring convergence is performed using automatic parameter selection. For a 3 μm microsphere, convergence of the calculation was achieved by including multipoles with an orbital angular momentum number of up to 21 and an azimuthal number of up to 20. Furthermore, the method uses the Extended Boundary Condition Methods to model light scattering by particles on substrates. The refractive index of SiO_2 was taken from ref. [47] and of silver from ref. [48]. A 3 μm diameter microsphere placed on a glass substrate, was illuminated using a p-polarized plane wave at an angle of 20° with respect to the substrate. The wavelength range of input light was 500–750 nm and the scattered light was integrated in the upper hemisphere with different polar angular ranges to get the scattering intensity to mimic the collection of the light using an objective lens.

Figure 2a shows the variation of the mode profile and linewidth for different collection angles. For smaller collection angles (0°–15°) the observed modes have very large linewidths. However, when the collection angles are increased (45°–60°), sharper modes are observed, which are distinct and are characterized by TE and TM modes. At larger angles such as between 60°–75°, the mode linewidth broadens because of the inclusion of the excitation light. Specifically, the intensity of the TM modes starts to decrease whereas the TE modes become much sharper at higher angles. This shows that distinct modes from the microsphere outcouple in different directions with varying intensity.

To further understand this phenomenon, we calculated the Mie modes as a function of NA of the objective lens (Figure 2b). With lower collection NAs (0.10 and 0.25), multiple modes get merged and appear as a single peak with broader linewidth. For 0.50 NA, only the TM modes are visible but with very broad linewidth. At higher NAs, such as 0.70 and 0.85 distinct TE and TM modes with low linewidth appear where the TE modes are relatively more intense than TM modes. For a nominal NA of 0.70, the calculated linewidth for the TE (TM) mode at 654 nm (638 nm) is 3.8 nm (7.5 nm) or 11 meV (22 meV).

Finally, to better understand the linewidth variation as a function of scattered wavevectors, we calculated the energy-momentum[49] image of the light scattered by the microsphere by dispersing the angular wavevectors along $k_y/k_0 = 0$ line with respect to the wavelengths as shown in Figure 2c. For this, the Fourier plane image of the scattered light from the microsphere was calculated for a range of input wavelengths, giving the radiation pattern in terms of azimuthal and polar angles, which can be expressed as the in-plane wavevector components k_x/k_0 and k_y/k_0. To obtain the dispersion of the scattered light, we extracted a one dimensional cut of the Fourier plane image along a fixed $k_y/k_0 = 0$ line and plotted the intensity as a function of k_x/k_0 (ranging from 0 to 1) and wavelength. The choice of $k_y = 0$ corresponds to the central cross-section of the momentum space,

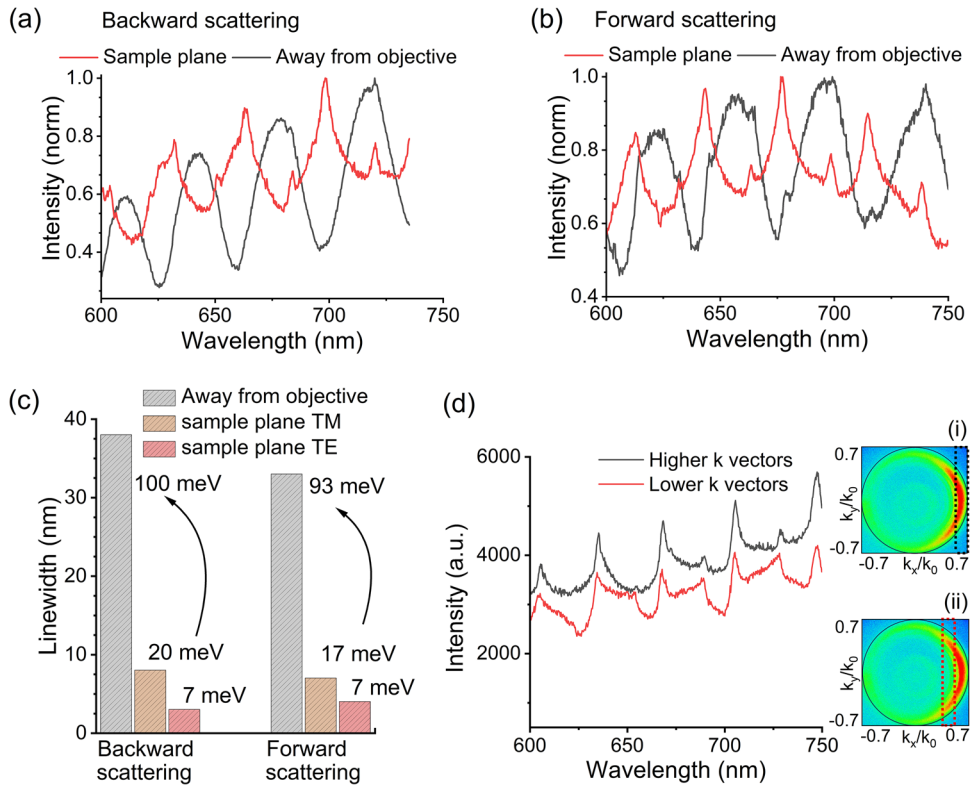

Figure 3. Experimentally observed Mie modes of a 3μm microsphere placed on a glass substrate upon excitation in a slant angle configuration. a,b) Mie modes observed by collecting the scattered light on the air (glass) side in backscattered (forward) configuration when the microsphere gives the sharpest modes (red line) and when the sample plane was moved away from the objective lens (black line). c) Bar plot of the variation of the observed linewidths of the Mie modes upon moving the microsphere away or at the sample plane of the objective lens. The FWHM of the modes showing that the observed modes can have different linewidths depending on the angular region of the scattered light that is collected by the objective lens. d) Momentum resolved Mie modes by projecting the Fourier plane image onto the spectrometer slit. The black (red) curve show the spectrum collected by projecting the higher (lower) k-values of the Fourier plane image where the Mie modes are most intense (less intense).

representing propagation in a single in-plane direction and excluding off axis contributions.

In general, TM modes exhibit broader linewidths than TE modes. This difference arises because TE modes have their electric field predominantly tangential to the substrate surface, resulting in weaker coupling to substrate modes.[24] In contrast, TM modes have a substantial radial (normal) electric field component, which couples more efficiently to the substrate. This enhanced coupling increases energy leakage into the substrate, leading to higher losses and thus broader spectral peaks than TE modes. Even for an isolated resonator, the linewidths of TM are larger than TE modes, because of the more radiative nature of the TM modes. However, the presence of a substrate preferentially further broadens the TM mode linewidth. Furthermore, Figure 2a–c shows that TM modes dominate at smaller collection angles, while both TE and TM modes appear at larger angles, with the TE mode becoming increasingly sharp. This trend can be understood from the directional nature of Mie scattering and the field orientation of the modes. The predominantly radial electric fields of the TM modes, results in stronger scattering at smaller angles. However, at larger angles, the overall Mie scattering intensity decreases, and the TM contribution becomes much weaker. In contrast, the tangential electric fields of the TE modes, scatter more efficiently at larger angles. As the collection angle increases, more TE mode intensity is collected resulting in the sharpens the of TE modes.

To demonstrate this effect, we performed experiments with a 3μm microsphere placed on a glass substrate and illuminated it with white light in an oblique angle excitation configuration at ≈20° with respect to the substrate. The scattered light was collected using an objective lens of 60×,

0.70 NA either from the upper hemisphere (backward scattering configuration) or in the lower hemisphere (forward scattering configuration). **Figure** 3a shows the Mie spectrum from the microsphere collected from the air side in the backward scattering configuration. We observed that the microsphere modes have low linewidth when the microsphere was placed near the sample plane of the microscope. This is due to the collection of scattered light from the microsphere with larger numerical aperture (0.7 NA) objective lens. Distinct resonances (both TE and TM) with narrow linewidths are observed and the spectrum fairly matches with the numerically calculated Mie scattering spectrum for 0.70 NA.

The linewidths of the TM and TE modes present at 700 and 720 nm are 8 nm (20 meV) and 3 nm (7 meV), respectively, which is very close to the values of the mode linewidth that are observed in the numerical calculations. However, when the microsphere was shifted away from the objective lens, the mode linewidth

increases drastically. This is expected because only the scattered light from the microsphere at the lower angles (near the $k_x/k_0 = k_y/k_0 = 0$) enters the objective lens. The bar plot in Figure 3c shows the change in the linewidth to 38 nm (100 meV) from 8 nm (20 meV) (TM) and 3 nm (7 meV) (TE) upon moving the microsphere away from the objective lens. Furthermore, the radial electric field nature of the TM modes leads to an enhanced coupling with the substrate. This increases the energy leakage into the substrate leading to higher losses and thus redshifted TM peaks at the lower angles. This shows that different collection angles can show an order of magnitude difference in the observed linewidth of microresonators. In addition, the observed Mie modes are also sensitive to the lateral position of the resonator at the sample plane as it changes the coupling of different modes into the objective lens, leading to variations in their intensities (see Supporting Information S3).

Furthermore, we performed similar experiment of probing Mie modes but in the forward direction, where the light was collected from the glass side. For this, the microsphere was placed on the glass coverslip and the white light was incident from the top side. We used the same dry 60×,

0.70 NA objective lens for the collection of the Mie modes. The objective lens has a correction collar to account for the thickness of the glass coverslip used in the experiments. Similar to the air side collection, in the glass side collection of the Mie modes, moving the microsphere away from the objective lens increases the linewidth of the modes (shown in Figure 3b). Even in this case, the observed linewidths can change from 33 nm (93 meV) to 7 nm (17 meV) (TM mode) and 3 nm (7 meV) (TE mode) depending on the location of the microsphere with respect to the objective lens, as shown in the bar plot in Figure 3c.

The observed dependence of the mode linewidths on the collection geometry in both backward and forward scattering (Figure 3a–c) indicates that angular filtering plays a crucial role in determining the measured spectral features. Since different scattering angles correspond to different momentum components of the emitted light, the numerical aperture and the angular acceptance of the detection optics directly influence the measured Mie spectrum. To investigate this effect more systematically, we performed momentum-resolved spectroscopy on a microsphere fixed at the sample plane. By imaging the Fourier plane onto the entrance slit of the spectrometer and selecting specific k-space regions, we could isolate contributions from different angular ranges. A 200 µm slit width was used to define the momentum selection (see Supporting Information S2 for experimental setup for momentum-resolved spectroscopy). The black curve in Figure 3d corresponds to higher angle (larger k-values) collection, which shows significantly narrower modes compared to the red curve obtained from lower angle (smaller k-values) collection. In both cases, the full k_y/k_0 range was integrated for the chosen k_x/k_0. This confirms that the sharpest modes predominantly scatter at higher angles, which is consistent with the NA dependent linewidth narrowing seen in Figure 3a–c, and demonstrates that momentum-resolved spectroscopy is an effective approach for selectively probing these modes under far-field excitation.

The above results show that to collect sharper modes, high NA lens should be used. However, experimentally, in the slant angle excitation configuration, the light is collected from the top side objective lens, with a large working distance, which also limits the NA of the lens that can be used under this dark-field spectroscopy configuration. To address this challenge, we demonstrate that metallic substrates can redistribute the scattered light wavevectors, particularly those emitted at high angles toward lower angles accessible to low-NA objectives. We show a similar effect in the collection of the modes of dielectric SiO_2 nanospheres where the metallic substrate can increase the collection efficiency of the higher order modes (TE_{11}) in the visible regime.

Figure 4a,b shows the calculated Fourier plane image of the scattered light from a 3 µm diameter microsphere placed on a glass substrate and a metallic substrate (silver film of 40 nm thickness), respectively. The microsphere was illuminated at 20° with respect to the substrate. The Fourier plane images show enhancement in the scattered intensity and also the redistribution of the scattered wavevectors toward the lower angles in the case of metallic substrate. The Fourier plane images are calculated in the upper hemisphere in the backscattered configuration. Intensity cross-cuts (Figure 4c) along the $k_y/k_0 = 0$ line in Figure 4a,b show that the scattering (for both TE and TM modes) is more intense at lower k values in the case of metallic substrate as compared to the glass substrate, where the scattering is prominent at higher k values. To compare the effect of the metallic substrate on the scattered Mie modes as compared to the glass substrate, we calculate the collection efficiency of the modes as a function of the numerical aperture of the collection objective lens. To calculate the collection efficiency, for each set of incident wavelengths the scattered spectrum of the Mie modes was calculated. After identifying the modes (TE and TM), the corresponding Fourier plane images were computed for each mode (over a range of wavelengths) within the upper half space, covering polar angles from 0° to 90° (corresponding to NA = 0 to 1). The collected intensity was then obtained by integrating the angular distribution from 0° to a specified polar angle, or equivalently from NA = 0 to the target NA. Here, 100 % collection efficiency refers to the total power emitted into the upper hemisphere, which in an ideal case can be collected by an objective lens of NA = 1. The collection efficiency is defined as the ratio of the power collected with a given NA to the power collected with NA = 1. Only the emission into the upper hemisphere was considered in the analysis. This shows that for a metallic substrate wavevector shifting can improve the collection efficiency of Mie modes for a given input angle and collection numerical aperture. The improvement is small when using a low NA lens, but for high NA lenses the collection efficiency can reach 80%, compared to around 60% for glass substrates. See Supporting Information S4 for experimentally obtained Mie modes of a 3 µm microsphere placed on a metallic mirror (thin silver film coated on a glass substrate). Placing the microsphere on the metallic substrate leads to a broadening of the TM modes, while the TE mode linewidth remains similar. Specifically, the TM mode linewidth increases from ≈8 nm (20 meV) to ≈10.4 nm (29 meV), whereas the TE mode linewidth stays around ≈3 nm (7 meV). This broadening of the TM modes arises from their stronger interaction with the metallic substrate, due to the predominantly radial nature of their electric field.

Finally using the same concepts and methodology, we show that metallic substrates can also increase the collection efficiency of the modes of dielectric nanospheres. Small sized low index dielectric particles support higher order electric and magnetic Mie modes in the visible regime, but the scattering efficiency is

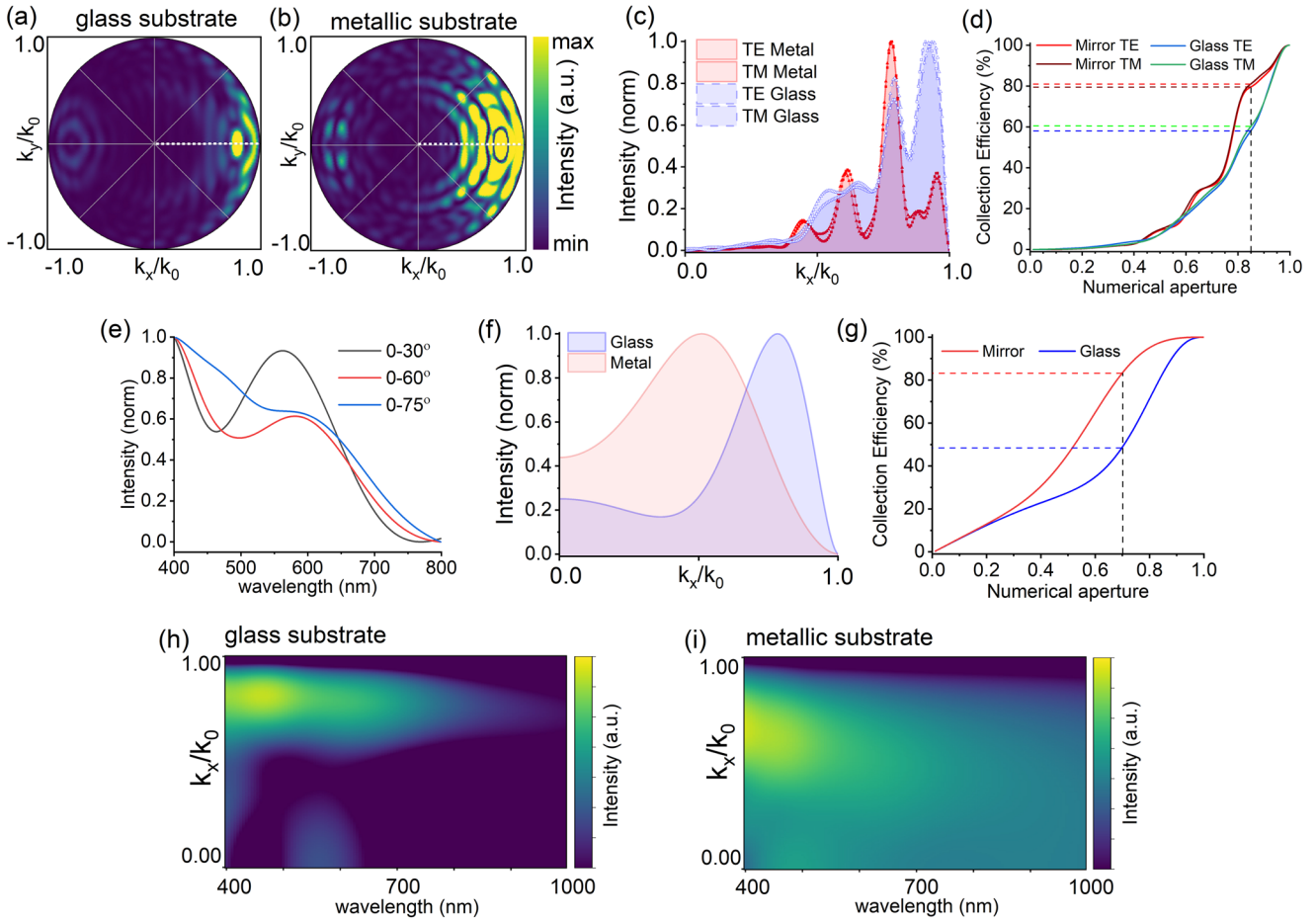

Figure 4. Effect of metallic substrate on the Mie modes far-field patterns and collection efficiency. a,b) Calculated Fourier plane image of the scattered light from a 3μm microsphere placed on a glass and metallic substrate respectively. c) Intensity cross-cut along the $k_y/k_0 = 0$ line in (a) and (b) showing the redistribution of Mie modes (TE and TM) towards the lower angles in case of metallic substrate. d) Collection efficiency increment of the modes in case of metallic substrate as a function of NA. e) Calculated scattering spectra of a 450 nm SiO_2 nanosphere showing a TE_{11} mode, for different collection range. Collection of the excitation light screens the scattering spectrum. f) Intensity distribution of the TE_{11} mode in the case of metallic and glass substrate showing the redistribution towards the lower angles while using metallic substrate. g) Collection efficiency increment of the mode when using a metallic substrate. h,i) Energy-momentum images showing the redistribution of the TE_{11} mode emission towards lower angles while using metallic substrate for full scattering wavelength range.

very low. This low scattering efficiency makes it difficult to detect and further use it for applications. However, attempts have been made to increase the scattering and collection efficiency by using metallic dressing as a top coating on the particles and modifying the Mie modes, as shown in ref. [33]. Herein we focus on redistributing the wavevectors of the scattered Mie modes by using metallic substrates, without any metallic coating on top which can alter the dielectric nature of the nanospheres. This wavevector redistribution increase the collection efficiency of the modes for a given numerical aperture of the objective lens. Figure 4e shows the calculated scattering spectrum of a 450 nm dielectric SiO_2 nanosphere placed on a glass substrate. The nanosphere size was selected to have Mie modes (TE modes) in the visible regime.[24,33] The nanosphere was excited with a p-polarized light at 30° with respect to the substrate and the scattered light was collected into the air side to get the intensity in the backscattering configuration. The mode linewidth of the TE_{11} mode changes slightly with a change in the collection angles. However, if the collected signal includes any of the incoming unscattered excitation light (as in the 0–75° range, blue curve), the mode is no longer visible. This shows that to get sharper modes in low refractive index dielectric particles, the incoming light should be completely removed by using very low NA collection angle, but this makes the collection intensity of the mode further weaker. We show that metallic substrate can redirect the emission towards the lower collection angles (Figure 4f, cross-cuts along the $k_y/k_0 = 0$ line of Fourier plane images of scattered light) which increases the collection efficiency of the mode. See supporting information S5 for the calculated Fourier plane image of the scattered mode form the nanosphere placed on a glass and metallic substrate. For a nominal NA of 0.70, the collection efficiency can increase from ≈50% to ≈80% as shown in the Figure 4g. This is made possible by the redistribution of the wavevector of the scattered mode in the case of metallic substrate as shown in the energy-momentum image where the mode spectrum is plotted along the wavevectors of the scattered light for both glass and

metallic substrate (Figure 4h,i). The metallic substrate redistributes the emission throughout the objective lens, which was however mainly confined at higher angles in the case of glass substrates. This makes the collection intensity to increase without relying on high NA lenses which can screens the modes. This improvement comes from the way a metallic substrate changes the wavevector distribution of the scattered mode, conceptually similar to k-space translation strategies used in metasurface holography[50] or metallic-dielectric antenna.[23] In the energy-momentum images (Figure 4h,i), the mode from the metallic substrate is spread more evenly across all collection angles, whereas for the glass substrate it is concentrated mainly at higher angles. This redistribution allows more of the mode light to be collected even with a lower NA lens, avoiding the need for very high NA optics that can otherwise obscures the mode because of inclusion of the unscattered excitation light.

3. Conclusion

In conclusion, we have demonstrated the influence of the numerical aperture (NA) of the objective lens on the observation of Mie mode profiles and linewidths in low refractive index microspheres. Our findings show that Mie modes outcouple at varying angles, with the amplitudes and resulting linewidths dependent on the NA of the collection optics. Furthermore, we show that metallic substrates act as optical antennas that redistribute the scattered wavevectors of Mie modes toward lower angles, thereby enhancing collection efficiency with low-NA objectives. A similar effect is observed for dielectric nanospheres, where the mode collection efficiency increases from 50% on a glass substrate to 80% on a metallic substrate due to this redistribution. Techniques such as back focal plane filtering can suppress contributions from low-k vectors and mode mixing, leading to more accurate observation of Mie modes. Given the growing interest in using dielectric microspheres and nanospheres as soft cavities for applications in lasing, sensing, and strong coupling, where linewidth is a key parameter, our results underscore the importance of accounting for detection geometry and substrate effects. Future work should extend these approaches to high refractive index nanoparticles, which support multiple electric and magnetic modes in the visible regime, offering further insights into the role of collection configuration in Mie mode analysis.

Supporting Information

Supporting Information is available from the Wiley Online Library or from the author.

Acknowledgements

T.F. thanks the Gordon and Betty Moore Foundation for funding support, the John Fell Fund, and the Oxford Martin School. S.T. acknowledges UK Research and Innovation (UKRI) under the UK government's Horizon Europe funding guarantee (EP/Z53464X/1). The authors thank Prof. Robert A. Taylor for support with experimental methodology, Amos Egel for SMUTHI codes, and Ryo Mizuta Graphics for 3D Blender optical components.

Conflict of Interest

The authors declare no conflict of interest.

Data Availability Statement

The data that support the findings of this study are available from the corresponding author upon reasonable request.

Keywords

dark-field spectroscopy, dielectric cavities, Fourier plane imaging, Mie resonances

Received: May 7, 2025
Revised: August 16, 2025
Published online:

[1] Y.-C. Lee, Y.-L. Ho, B.-W. Lin, M.-H. Chen, D. Xing, H. Daiguji, J.-J. Delaunay, *Nat. Commun.* **2023**, *14*, 6458.
[2] S. I. Azzam, K. Chaudhuri, A. Lagutchev, Z. Jacob, Y. L. Kim, V. M. Shalaev, A. Boltasseva, A. V. Kildishev, *Laser Photonics Rev.* **2021**, *15*, 2000411.
[3] J. Garcia-Guirado, M. Svedendahl, J. Puigdollers, R. Quidant, *Nano Lett.* **2019**, *20*, 585.
[4] G. P. Zograf, M. I. Petrov, S. V. Makarov, Y. S. Kivshar, *Adv. Opt. Photonics* **2021**, *13*, 643.
[5] A. I. Chernov, M. A. Kozhaev, D. O. Ignatyeva, E. N. Beginin, A. V. Sadovnikov, A. A. Voronov, D. Karki, M. Levy, V. I. Belotelov, *Nano Lett.* **2020**, *20*, 5259.
[6] J. Amboli, B. Gallas, G. Demésy, N. Bonod, *Opt. Express* **2023**, *31*, 43147.
[7] S. Bidault, M. Mivelle, N. Bonod, *J. Appl. Phys.* **2019**, *126*, 9.
[8] H.-J. Lee, K.-A. Hyun, H.-I. Jung, *Appl. Phys. Lett.* **2014**, *104*, 2.
[9] Y. Li, X. Liu, B. Li, *Light: Sci. Appl.* **2019**, *8*, 61.
[10] D. Ha, C. Gong, M. S. Leite, J. N. Munday, *ACS Appl. Mater. Interfaces* **2016**, *8*, 24536.
[11] K. Bi, D. Yang, J. Chen, Q. Wang, H. Wu, C. Lan, Y. Yang, *Photonics Res.* **2019**, *7*, 457.
[12] P. Moitra, B. A. Slovick, W. Li, I. I. Kravchencko, D. P. Briggs, S. Krishnamurthy, J. Valentine, *Acs Photonics* **2015**, *2*, 692.
[13] T. Zhang, X. Chen, Y. Thakur, B. Lu, Q. Zhang, J. Runt, Q. Zhang, *Sci. Adv.* **2020**, *6*, eaax6622.
[14] N. Toropov, G. Cabello, M. P. Serrano, R. R. Gutha, M. Rafti, F. Vollmer, *Light: Sci. Appl.* **2021**, *10*, 42.
[15] X. Jiang, A. J. Qavi, S. H. Huang, L. Yang, *Matter* **2020**, *3*, 371.
[16] W. Mao, Y. Li, X. Jiang, Z. Liu, L. Yang, *Light: Sci. Appl.* **2023**, *12*, 247.
[17] S. Zhou, Y. Deng, W. Zhou, M. Yu, H. Urbach, Y. Wu, *Appl. Phys. B* **2017**, *123*, 1.
[18] T. X. Hoang, Y. Duan, X. Chen, G. Barbastathis, *Opt. Express* **2015**, *23*, 12337.
[19] S. Laskar, A. C. Dakshinamurthy, S. Chithamallu, C. Sudarshan, C. Sudakar, *Opt. Lett.* **2023**, *48*, 2643.
[20] X. Liu, S. T. Ha, Q. Zhang, M. de la Mata, C. Magen, J. Arbiol, T. C. Sum, Q. Xiong, *ACS nano* **2015**, *9*, 687.
[21] X. Li, K. Wang, M. Chen, S. Wang, Y. Fan, T. Liang, Q. Song, G. Xing, Z. Tang, *Adv. Opt. Mater.* **2020**, *8*, 2000030.
[22] R. Duan, Z. Zhang, L. Xiao, X. Zhao, Y. T. Thung, L. Ding, Z. Liu, J. Yang, V. D. Ta, H. Sun, *Adv. Mater.* **2022**, *34*, 2108884.
[23] A. B. Vasista, S. Tiwari, D. K. Sharma, S. K. Chaubey, G. P. Kumar, *Adv. Opt. Mater.* **2018**, *6*, 1801025.
[24] C. F. Bohren, D. R. Huffman, *Absorption and Scattering of Light by Small Particles*, John Wiley & Sons, Hoboken, NJ **2008**.
[25] M. Khoury, H. Quard, T. Herzig, J. Meijer, S. Pezzagna, S. Cueff, M. Abbarchi, H. S. Nguyen, N. Chauvin, T. Wood, *Adv. Opt. Mater.* **2022**, *10*, 2201295.

[26] S. Kruk, Y. Kivshar, *Acs Photonics* **2017**, *4*, 2638.
[27] I. Staude, J. Schilling, *Nat. Photonics* **2017**, *11*, 274.
[28] F. Biccari, T. Hamilton, A. Ristori, S. Sanguinetti, S. Bietti, M. Gurioli, H. Mohseni, *Part. Part. Syst. Charact.* **2020**, *37*, 1900431.
[29] Z. Wang, W. Guo, L. Li, B. Luk'Yanchuk, A. Khan, Z. Liu, Z. Chen, M. Hong, *Nat. Commun.* **2011**, *2*, 218.
[30] I. V. Minin, O. V. Minin, I. A. Glinskiy, R. A. Khabibullin, R. Malureanu, A. V. Lavrinenko, D. I. Yakubovsky, A. V. Arsenin, V. S. Volkov, D. S. Ponomarev, *Opt. Lett.* **2020**, *45*, 3244.
[31] S. Si, T. Kaneko, L. Xu, H. Luo, H. Nakajima, N. Kasai, K. Uchiyama, D. Wu, H. Zeng, *Biosens. Bioelectron.* **2022**, *218*, 114791.
[32] S. H. Huang, X. Jiang, B. Peng, C. Janisch, A. Cocking, Ş. K. Özdemir, Z. Liu, L. Yang, *Photonics Res.* **2018**, *6*, 346.
[33] J. Zhou, A. Panday, Y. Xu, X. Chen, L. Chen, C. Ji, L. J. Guo, *Phys. Rev. Lett.* **2018**, *120*, 253902.
[34] O. V. Minin, I. V. Minin, S. Zhou, *arXiv preprint arXiv:2204.09175* **2022**.
[35] Z. Wang, B. Luk'yanchuk, L. Yue, B. Yan, J. Monks, R. Dhama, O. V. Minin, I. V. Minin, S. Huang, A. A. Fedyanin, *Sci. Rep.* **2019**, *9*, 20293.
[36] A. B. Vasista, W. L. Barnes, *Nano Lett.* **2020**, *20*, 1766.
[37] A. B. Vasista, E. J. Dias, F. J. Garcia de Abajo, W. L. Barnes, *Nano Lett.* **2022**, *22*, 6737.
[38] M. B. Price, K. Lewellen, J. Hardy, S. M. Lockwood, C. Zemke-Smith, I. Wagner, M. Gao, J. Grand, K. Chen, J. M. Hodgkiss, E. Le Ru, N. J. L. K. Davis, *J. Phys. Chem. Lett.* **2020**, *11*, 7009.
[39] J. Wang, Q. Hao, Y. Yin, L. Ma, O. G. Schmidt, *Phys. Status Solidi (b)* **2019**, *256*, 1800379.
[40] Z. Geng, J. Theenhaus, B. K. Patra, J.-Y. Zheng, J. Busink, E. C. Garnett, S. R. Rodriguez, *ACS photonics* **2021**, *8*, 1271.
[41] M. W. Knight, J. Fan, F. Capasso, N. J. Halas, *Opt. Express* **2010**, *18*, 2579.
[42] J. A. Fan, K. Bao, J. B. Lassiter, J. Bao, N. J. Halas, P. Nordlander, F. Capasso, *Nano Lett.* **2012**, *12*, 2817.
[43] B. Redding, E. Marchena, T. Creazzo, S. Shi, D. W. Prather, *Opt. Lett.* **2010**, *35*, 998.
[44] N. Riesen, T. Reynolds, A. François, M. R. Henderson, T. M. Monro, *Opt. Express* **2015**, *23*, 28896.
[45] A. Egel, K. M. Czajkowski, D. Theobald, K. Ladutenko, A. S. Kuznetsov, L. Pattelli, *J. Quant. Spectrosc. Radiat. Transfer* **2021**, *273*, 107846.
[46] A. Egel, D. Theobald, Y. Donie, U. Lemmer, G. Gomard, *Opt. Express* **2016**, *24*, 25154.
[47] I. H. Malitson, *J. Opt. Soc. Am.* **1965**, *55*, 1205.
[48] P. B. Johnson, R.-W. Christy, *Phys. Rev. B* **1972**, *6*, 4370.
[49] C. M. Dodson, J. A. Kurvits, D. Li, R. Zia, *Opt. Lett.* **2014**, *39*, 3927.
[50] Z. Liu, H. Gao, T. Ma, V. Ray, N. Liu, X. Zhang, L. J. Guo, C. Zhang, *Elight* **2024**, *4*, 7.